World Academy of Science, Engineering and Technology
International Journal of Civil and Environmental Engineering
Vol:5, No:7, 2011

Simulating Pathogen Transport within a Naturally Ventilated Hospital Ward

C. A. Gilkeson, C. J. Noakes, P. A. Sleigh, M. A. I. Khan and M. A. Camargo-Valero

***Abstract*—**Understanding how airborne pathogens are transported through hospital wards is essential for determining the infection risk to patients and healthcare workers. This study utilizes Computational Fluid Dynamics (CFD) simulations to explore possible pathogen transport within a six-bed partitioned Nightingale-style hospital ward.

Grid independence of a ward model was addressed using the Grid Convergence Index (GCI) from solutions obtained using three fully-structured grids. Pathogens were simulated using source terms in conjunction with a scalar transport equation and a RANS turbulence model. Errors were found to be less than 4% in the calculation of air velocities but an average of 13% was seen in the scalar field.

A parametric study of variations in the pathogen release point illustrated that its distribution is strongly influenced by the local velocity field and the degree of air mixing present.

***Keywords*—**Natural, Ventilation, Pathogen, Transport

I. Introduction

THE airborne transmission of pathogens such as tuberculosis and strains of influenza pose a great threat to human health. This is especially the case in healthcare environments such as hospital wards because the patients they house often have weakened immune systems, making them more susceptible to acquiring infections. In order to reduce the infection risk within hospital wards though improved design and development of engineering solutions, the movement of pathogens must be characterized.

The notion that airborne pathogens could travel large distances and remain in the air for long periods of time was first entertained in the early 1930's. During this period two pioneering studies [1], [2] showed that organisms released in the basement of large three-storey buildings could be transported to the upper levels. The explanation for this was that the internal air currents had conveyed the microorganisms throughout the building, which illustrates the extent to which airborne transmission can spread and disperse these organisms. Whilst the airborne route of transmission has been confirmed experimentally, it is inherently difficult to measure due to the small particle sizes involved which are typically on the order of 0.1 – 10 μm in diameter. Tracking such particles experimentally through indoor spaces presents an extraordinary challenge.

Carl Gilkeson is a Postdoctoral Research Fellow from the Pathogen Control Engineering Institute, School of Civil Engineering, University of Leeds, Leeds, UK, LS2 9JT.;
email: c.a.gilkeson@leeds.ac.uk)

However, the maturity of Computational Fluid Dynamics (CFD) is now such that this type of phenomenon can be studied in great detail. There are two approaches for simulating pathogens using CFD: (i) Lagrangian and (ii) Eulerian.

In the Lagrangian approach discrete particles are modeled, distributed and tracked throughout the flow field over time [3]. While this approach is based on the physics of particle motion, one drawback is that the specified particles may not travel through some regions of the flow [4], [5]. In contrast, the Eulerian method solves a scalar transport equation resulting in domain-wide scalar concentration distributions. In the context of aerobiology, this method is considered appropriate for respirable-sized particles (< 5 μm in diameter), known as droplet nuclei, that are assumed to remain airborne for long periods of time. Numerous studies have adopted this approach including simulated droplet nuclei dispersion [5] and prediction of microorganism kill rates under the influence of Ultraviolet Germicidal Irradiation (UVGI) [4]. The focus of the present study is to apply this Eulerian methodology by simulating pathogen transport in a naturally ventilated hospital ward.

II. Experimental Methodology

A recent experimental study into pathogen transport and ventilation inside a former Nightingale hospital ward (Fig. 1) demonstrated the effectiveness of natural ventilation in both an open ward and a modified space with partitions located between beds [6].

Fig. 1 Photograph of A-Block, St. Lukes Hospital, Bradford, UK

With a plan area of 9.75 m x 7.25 m, the internal volume of the ward is ~195m^3. A pulse-injection method was employed using CO_2 as a surrogate tracer to measure ventilation rates [6]. Results showed that under the influence of natural ventilation the air exchange rate varied from a minimum of 2 air changes per hour (ACH) up to 30 ACH. The variation of ventilation rates observed was attributable to the ambient wind speed and its direction.

During the experiments three top-hinged casement-type windows were opened on both sides of the building to induce a regime of span-wise cross-ventilation. Flow visualization via smoke sticks in the vicinity of the window openings confirmed that fresh air typically passed through the building by entering the West-facing windows and exiting through the East-sided ones. Flow direction was well-defined on the inlet windows and the mean flow showed a tendency to follow the contours of the opening, see Fig. 2 (a). These observations are used to specify suitable boundary conditions in the following section.

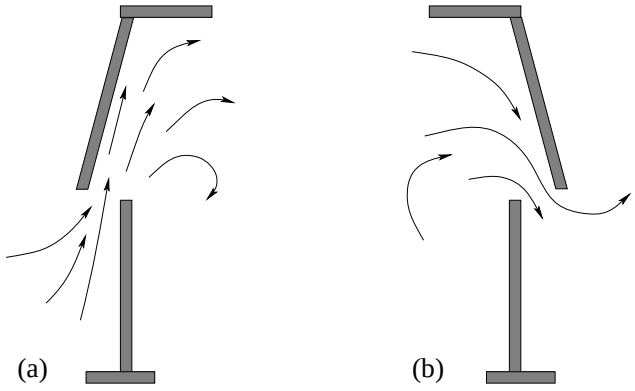

Fig. 2 Illustration showing the observed flow direction around (a) the inlet and (b) the outlet

III. CFD Methodology

A. Geometry and Boundary Conditions

Simulating natural ventilation inside a large building such as the one in question is extremely challenging due to the broad spectrum of time and length scales involved [6], [7]. As such, the present study is limited to steady-state simulations of the flow field for the internal air volume only. Generating a coupled internal-external flow field within the ward would represent a prohibitively large task and is thus beyond the scope of this investigation.

A CAD model of the internal air volume was produced using Gambit (Version 2.4). The ward consists of six inter-connected bays, each with a simplified bed and a full-height vertical partition between bays, see Fig. 3. Although the external air volume was neglected, the window apertures were accounted for which included faces representing the interface between the internal and external volumes (assuming fully-opened windows). By using this approach the angle at which air enters the building can be set to match that which was seen experimentally. These inlet faces were assigned velocity inlet boundary conditions with a velocity vector parallel to the upper (opened) face of the window.

On the opposing side of the ward, pressure outlets were placed in the window openings to exhaust the incoming airflow. As mentioned in Section I. the experimentally measured ventilation rates varied from 2 to 30 ACH, however, the average value was typically 4 to 8 ACH. Following this a decision was taken to use a value of 6 ACH in the simulations and this was done by assigning appropriate velocity magnitudes on the inlets, giving an equivalent airflow rate of 1170 m^3/h. The pressure outlet faces were assigned a constant pressure of -20 Pa which was consistent with experimental measurements taken using a low-range manometer (Testo 512, Testo Ltd, Alton, Hampshire, UK).

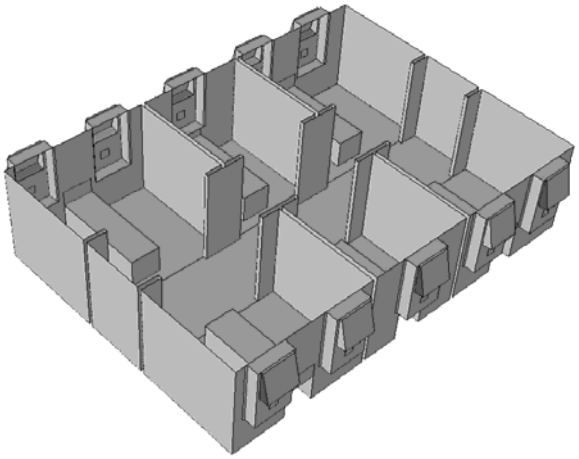

Fig. 3 CAD model of the Nightingale hospital ward showing vertical partitions between beds and recessed widow apertures.

Despite the fact that the model contains ten windows in total, only three pairs had air passing through them, namely: the central pair and those at either end of the ward.

B. Grid Independence

The sensitivity of computed solutions to the grid density was assessed using a rigorous grid independence study. Prior to grid generation in Gambit, the solution domain was decomposed into approximately 650 volumes to enable full control over the grid structure. Three fully-hexahedral grids were produced with the properties shown in Table. I.

TABLE I
GRID PROPERTIES

Grid Type	Grid Spacing (mm)	Total Cell Count
Coarse	25	1235429
Medium	35	3326216
Fine	49	9018918

Here, the grid refinement ratio (based on element edge lengths), r, was set to 1.4 which is greater than the recommended minimum value of 1.3 [8]. Initially, grid halving was attempted (i.e. r = 2) however, the coarse grid

had too few cells which led to convergence problems and thus gave a very poor solution which was inadequate. The chosen refinement ratio of 1.4 gave a good spread of cell counts from which to estimate the discretisation error. Some degree of grid stretching in the span-wise direction was necessary for all three grids to cater for the high flow gradients which were expected around the ends of the vertical partitions, see Fig. 4.

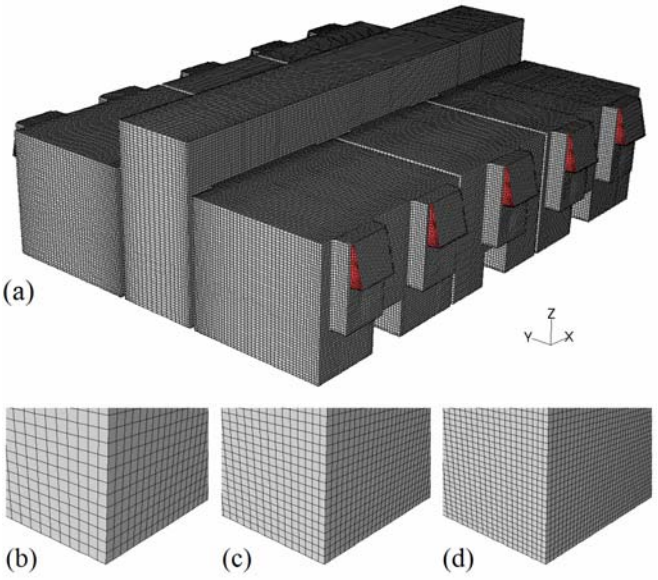

Fig. 4 Illustration of (a) the entire coarse grid structure and inset local grid density for (b) coarse, (c) medium and (d) fine grids respectively.

Solutions for continuity, momentum, and turbulence were computed on each grid using 2nd order discretisation and the standard k-ε turbulence model [9] in conjunction with standard wall functions. All simulations were run in parallel on an HPC cluster with 16 processors (2 x dual-quad core 2.26 Ghz Nahalem processors and 24 Gb of SDD RAM) using Fluent (Version 12.1). To avoid convergence error the simulations ran for 20,000 iterations with the default residual tolerance deliberately turned off. Analysis of the residual histories showed that convergence had occurred after 4200, 7000 and 14000 iterations for the coarse, medium and fine grid solutions respectively. In all of these simulations, absolute residual levels had dropped by over four orders of magnitude for continuity and ε, with a drop of between five and six orders of magnitude for k, and the three components of air velocity.

Next, the user-defined scalar transport equation was invoked together with a source term to represent a pathogen release. The source term was implemented with a user-defined function (UDF) which essentially specified a rate of release of a given scalar concentration (or pathogen), this emanating from a spherical volume (radius = 0.30 m) situated above one of the beds. Experience has shown that the scalar is best solved by itself on the converged flow field, thus the flow equations are turned off whilst the 2nd order scalar transport equation is solved. Convergence of the scalar took an additional 800 to 1500 iterations depending on grid type.

Having obtained solutions to the flow and scalar fields, grid independence was assessed in terms of relevant flow variables. Two quantities were of interest: (i) the normalized velocity magnitude, U/U_{max} and (ii) the normalized scalar concentration, $S/S_{max.}$. Both of these quantities are plotted along a span-wise line in the centre of the ward, passing through the centre of the source, see Fig. 5.

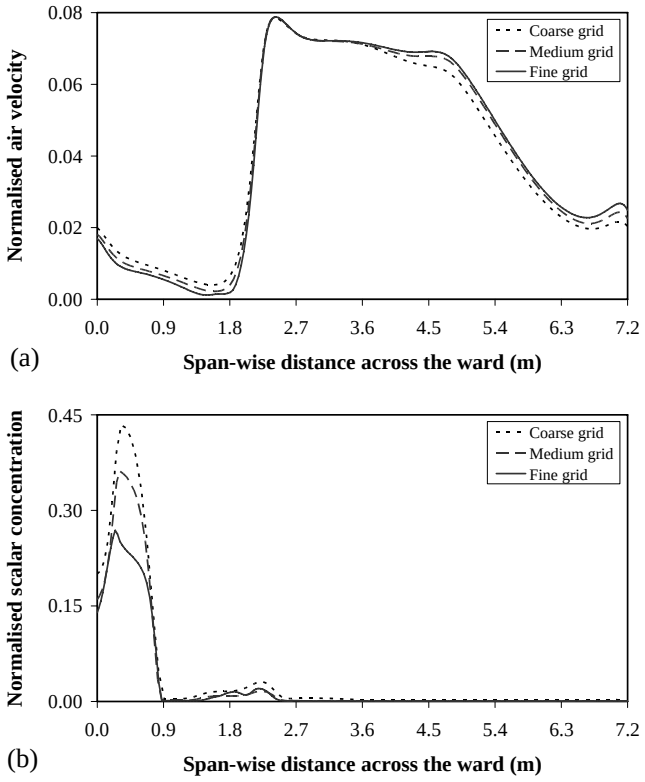

Fig. 5 Plots showing the distribution of (a) normalized air velocity and (b) normalized scalar concentration across the width of the building.

In terms of the air velocities, all three solutions follow the same general trend with very similar peak values occurring at the same point, Fig. 5(a). The distribution of the scalar concentration is much more sensitive to the grid spacing, especially near the source which occurs 0.5 m along the length of the ward, Fig. 5(b). Clearly the peak concentrations appear to be grid dependent in this region of the flow. However, further investigation showed that this sensitivity coincides with the centre of the spherical volume which emits the source. Furthermore, this dependency has a radius of influence which is almost the same as the radius of the source volume itself. Outside of this volume broadly similar scalar quantities are seen.

Although qualitative grid independence is evident in the medium-grid solutions, quantitative errors are useful in determining this more specifically. The Grid Convergence Index (GCI) [10] is suitable for calculating the discretisation

TABLE II
ESTIMATED GCI ERRORS

Air volume	E_V (%)	E_S (%)
Bay 1	2.25	23.36
Bay 2	0.56	21.37
Bay 3	3.40	4.49
Bay 4	0.38	11.50
Bay 5	2.99	9.82
Bay 6	0.67	12.25
Corridor	0.64	6.66

error based on the solutions from different grids. This technique also takes into account the grid spacing and the order of discretisation, p, making this a rigorous method for quantifying the uncertainty present in the CFD solutions. Table II shows calculated discretisation errors between the medium and fine grid solutions for quantities within each of the seven sub-volumes, namely, all six bays in addition to the corridor. Errors for (i) the normalized velocity magnitude, E_V, and (ii) the scalar concentration, E_S, were computed based on volume-averaged quantities in each of those volumes. The results follow a similar trend to that shown in Fig. 5 whereby small discretisation errors are observed in the air velocity magnitudes with a range of between 0.38% and 3.40%. There is an order of magnitude increase for the scalar quantities with values of between 4.49% and 23.36%, underlining the fact that the computed scalar field is much more sensitive to global grid refinement than the underlying flow field. Interestingly the errors in velocity magnitude are all less than 0.6% in the central corridor and on the east (outlet) side of the building (bays 2, 4 and 6), whereas the errors are more than four times greater in each of the west (inlet) bays. This suggests that the distribution of errors is such that they are generally greater on the inlet side of the building which is perhaps due to the fact that the flow is developing with higher gradients in those regions. The same cannot be said for the distribution of errors in the scalar field; no clear trend is evident. Clearly, CFD solutions of the scalar transport equation are much more sensitive to the grid spacing than the actual flow field. There may be some scope to minimize this sensitivity through grid adaption, particularly close to the source, however this aspect is not considered here.

IV. Results and Discussion

A. Flow Field

Following the grid independence study the medium-grid solution was investigated in more depth. This was considered sufficient enough to determine qualitative aspects of pathogen transport which is the primary focus of this paper. Fig. 6 shows relative velocity magnitude contours when viewed from above. The three inlet jets serve to mix the airflow within the ward but a heterogeneous velocity distribution is evident with a number of low-velocity 'dead' regions present. The observed asymmetry in the flow pattern is to be expected because the geometry of the ward was taken from a real building which is non-symmetric. Subtle differences such as the positioning of the windows relative to the partitions and variations in the width of each bay all contribute to the asymmetry present. This feature has implications for the computed scalar field which is discussed in the next section. The highest air velocities occur where the flow accelerates around the ends of the partitions. On the leeward side of these protrusions the lowest velocities are seen.

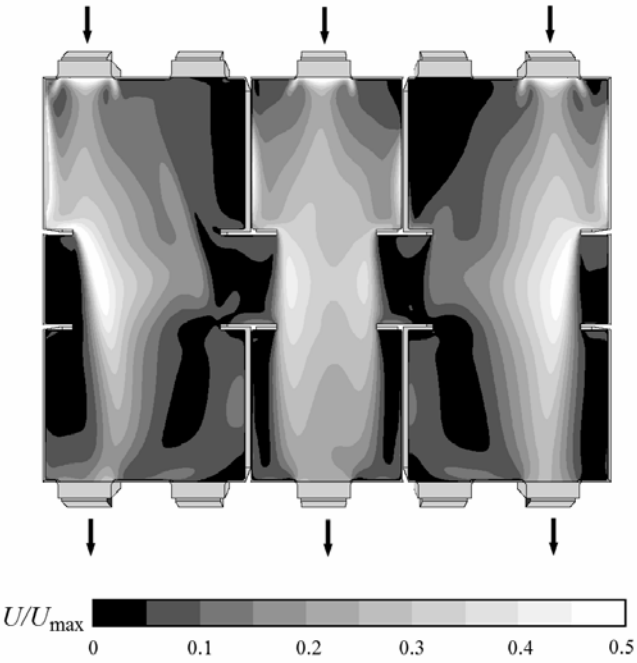

Fig. 6 Contour plot of relative velocity magnitude taken from a plane situated 2.2 m above ground level and viewed from above

Further investigation of the flow pattern is revealed using pathlines, see Figs. 7-9. In Fig. 7 a total of 275 pathlines are shown. Each of these is released from the velocity inlet face from within the window aperture of bay number 1, and allowed to travel a maximum of 2.5 m along each individual trajectory.

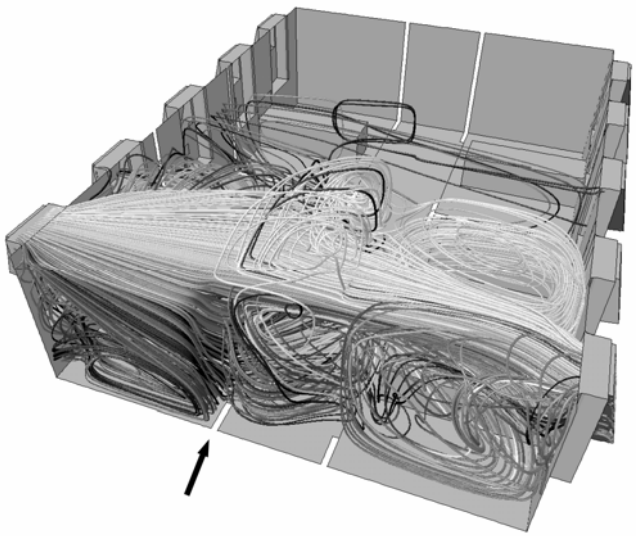

Fig. 7 Pathlines released from the inlet window in bay number 1, flow from left-to-right

Here, the flow is characterized by a column of air passing through the ward just below the ceiling. Some of the incoming fresh air at the South end of the bay is forced downwards and then back on itself due to the small partition present on the South wall (indicated by the arrow in Fig. 7). Whilst the majority of the pathlines are largely contained within the end two bays, some of them travel along the corridor and into the adjacent bays. Fig. 8 shows the flow pattern with pathlines originating from the inlet of the west-facing central bay. The flow structure here is dominated by a column of air which accelerates through the ward due to the constriction imposed by the ends of the partitions. This channeling effect lessens the amount of air mixing present in the centre of the ward.

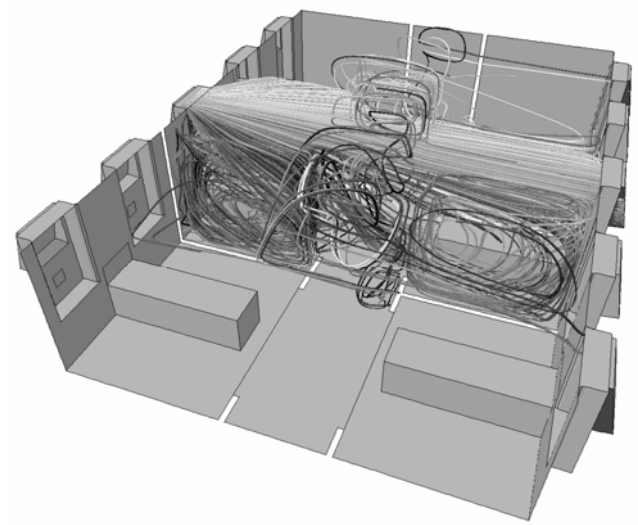

Fig. 8 Pathlines released from the inlet window in bay number 3, flow from left-to-right

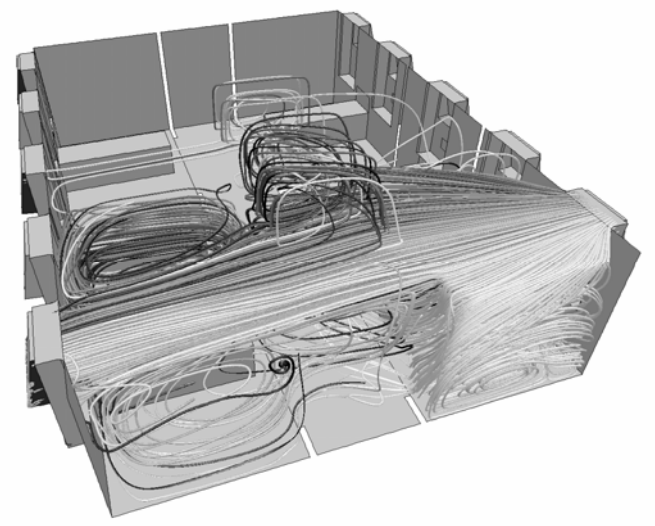

Fig. 9 Pathlines released from the inlet window in bay number 5, flow from right-to-left

The airflow structure at the far (North) end of the ward is shown in Fig. 9 (note that for clarity the orientation of this figure is different to Figs. 7 and 8, and the flow appears as right-to-left in this case). The positioning of the windows in these bays is such that the partitions are less effective at containing the flow and so a larger proportion of the incoming air passes directly across the ward.

B. Windward Pathogen Release

Next, the sensitivity of the source location on the simulated pathogen concentration levels is investigated. Fig. 10 shows the results for three cases with a windward-release i.e. for bays adjacent to the inlet windows. Figs. 10(a) and (d) highlight a substantial degree of mixing in bay number 1 which effectively contains the pathogen in a local vortical flow structure despite the cross-ward ventilation regime. Considering the central release, Figs. 10(b) and (e), the pathogen is transported directly across the ward to the opposing bay, thereby increasing the infection risk in this region (under these conditions). This is attributable to the substantially smaller width of the central bays as they gently constrict the flow, inducing a mild Venturi effect, leading to higher local air velocities and thus greater potential to transport the pathogen.

The result for the far-corner release shows a high level of mixing which spreads the pathogen throughout bay 5, Figs 10(c) and (f). There is some evidence of cross-ward transportation of the scalar, however the risk is substantially lower than that seen in the central bay.

C. Leeward Pathogen Release

Three further simulations considered leeward pathogen release i.e. pathogen sources adjacent to the outlet windows. With a source release from just above the bed in bay number 2, the pathogen is drawn towards the ground, at either side of the bed, see Figs. 11(a) and (d). Local recirculation patterns between the bed and the surrounding walls serve to contain the highest concentrations of the scalar and it is conceivable that the infection risk could be higher without partitions present.

Moving to the result for the leeward central release, the channeling effect already described is very effective at removing the pathogen from the window above the bed, Figs. 11(b) and (e). Interestingly the pathogen is initially drawn towards the centre of the ward before it turns back on itself prior to exiting. This is a consequence of a large, centrally-located re-circulatory flow pattern which is driven by the inlet jets. As the air moves across the ward just below ceiling-level, the ground-level flows oppose this, leading to a shearing effect and consequent recirculation.

For the far-corner leeward release, the pathogens is transported by the aforementioned circulatory flow pattern which sweeps it close to the ground and towards the opposing patient, see Figs. 7(c) and (f).

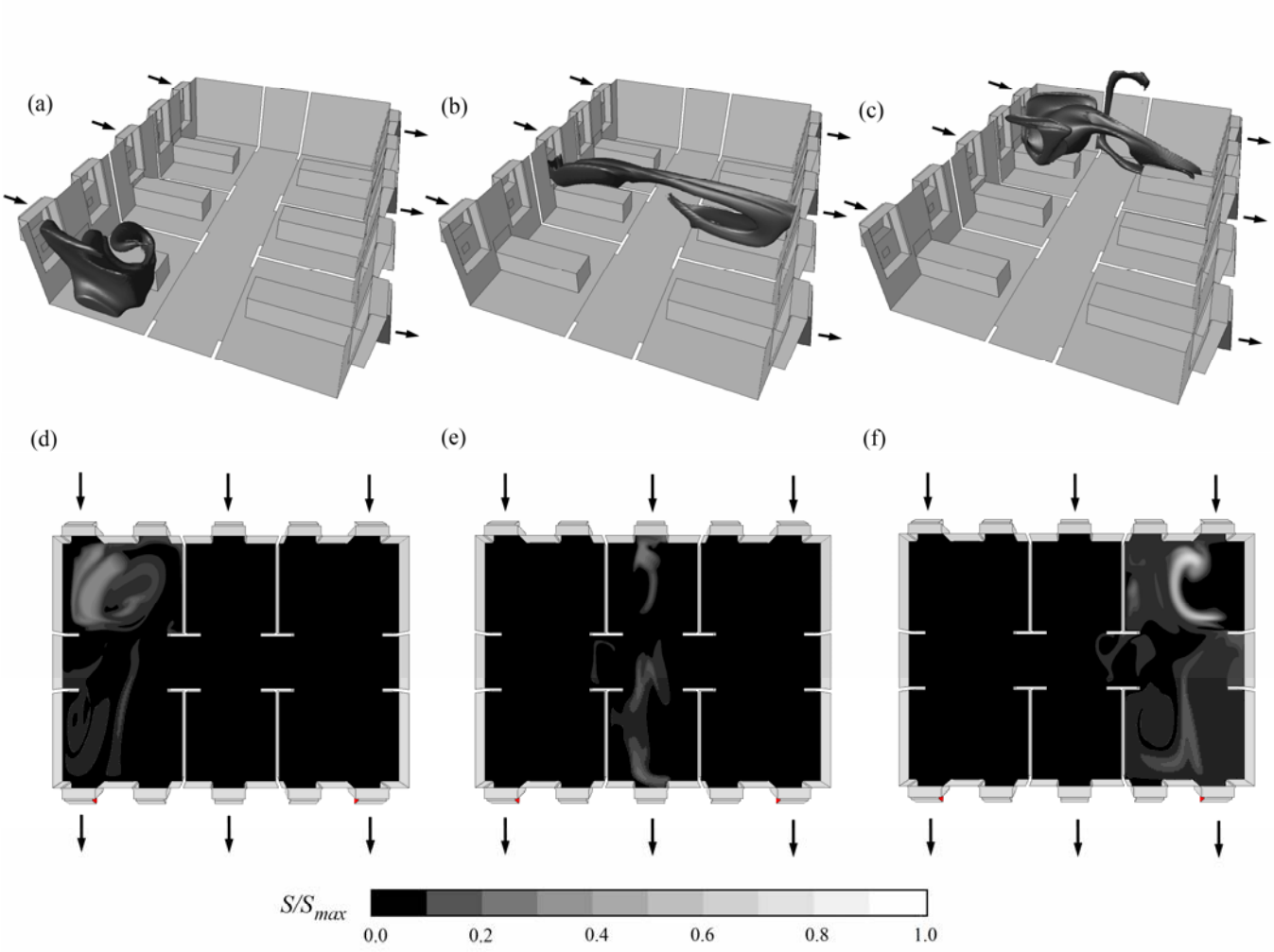

Fig. 10 Iso-surfaces for windward scalar release from (a) bay 1, (b) bay 3, (c) bay 5 and corresponding normalized scalar contour plots at patient head height (1.0 m above ground level) for (d) bay 1, (e) bay 3 and (f) bay 5

D. Discussion

The results presented in this paper demonstrate the viability of the Eulerian approach to simulating pathogen transport through a hospital ward. A thorough grid independence study highlighted a degree of sensitivity of the simulated pathogen concentration to the grid density, particularly near the source. This was attributable to local grid density which may be minimized through grid adaption in future studies.

In terms of the broader distribution of this pathogen, it was found to be sensitive to (i) the release point, (ii) characteristics of the flow field and (iii) the proximity of specific geometrical features such as the position of the windows and the partitions. Overall, the highest scalar concentrations occurred in slow-moving regions of the flow, whereas the lowest concentrations coincided with high-velocity columns of air which spanned the width of the building.

The results also suggest that the presence of trapped or standing vorticies may act as sinks to draw in the pathogen and keep it in one location (such as that shown in Fig. 10(a)). However such a flow feature is unlikely to remain stationary in a real environment and the influence of moving doors and people will play a significant role in modifying any generic flow patterns and thus pathogen transport.

The dispersion of the pathogen is generally less in the leeward release cases, compared to the windward ones. This is not unexpected given the cross-ventilation regime. Under these conditions leeward pathogenic release is less likely to travel as far because of the close proximity of the outlets.

Another interesting feature of the flow was the longitudinal asymmetry present in the pathogen distribution. Deeper investigation of this cited an interaction between the longitudinal window position and that of the partition ends. An implication of this is that obstructions occurring in between windward and leeward windows do modify the flow somewhat. This type of obstruction is likely to happen in the everyday operation of hospitals due to human activity and the effective barrier to pathogen transport.

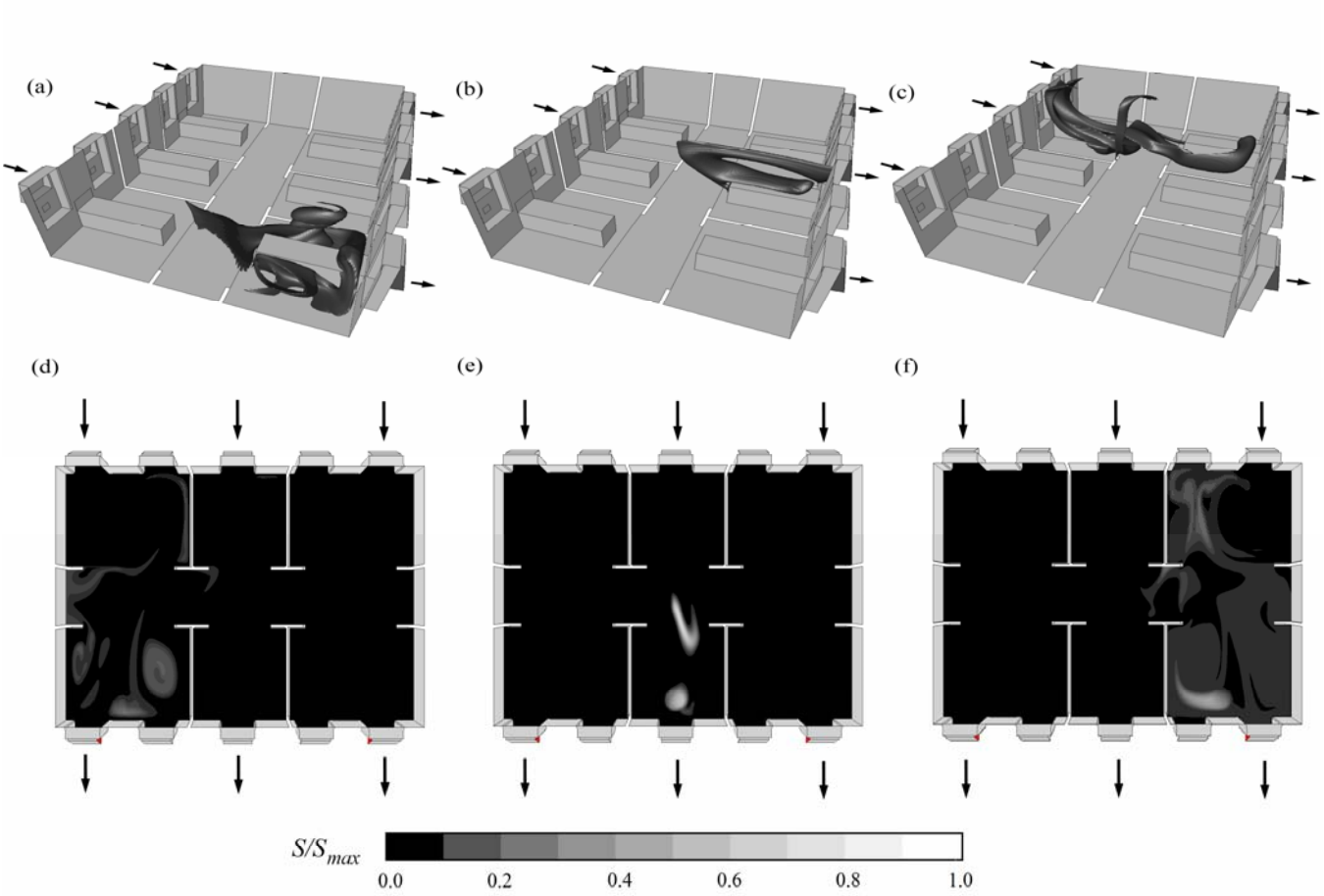

Fig. 11 Iso-surfaces for leeward scalar release from (a) bay 2, (b) bay 4, (c) bay 6 and corresponding normalized scalar contour plots at patient head height (1.0 m above ground level) for (d) bay 2, (e) bay 4 and (f) bay 6.

V. Conclusion

This investigation utilized the qualities of high-fidelity CFD simulation to study simulated pathogen transport in a partitioned hospital ward. Confidence in the accuracy of the simulations was drawn from the results of a rigorous grid independence study and behavior which concurred with experimental results. It was found that using a scalar transport equation in conjunction with the CFD solution was effective at visualizing pathogen transport throughout the domain. Although a number of trends were evident, further study is required to investigate the influence of important factors such as ventilation rate and variants of building geometry such as inter-bed spacing and ceiling height. Research is currently ongoing in this area.

References

[1] G. W. McCoy, "Psittacosis Among the Personnel of the Hygenic Laboratory," *The Journal of Infectious Diseases*, vol. 55, no. 2, pp. 156-167, September 1934.

[2] W. F. Wells, "Air-borne infection and sanitary control," *Journal of Industrial Hygiene*, vol. 17, pp. 253-257, 1935.

[3] A. Alani, I. E. Barton, M. J. Seymour, and L. C. Wrobel, "Application of Lagrangian particle transport model to tuberculosis (TB) bacteria dosing in a ventilated isolation room," *International Journal of Environmental Health Research*, vol. 11, pp. 219-228, 2001.

[4] C. J. Noakes, L. A. Fletcher, C. B. Beggs, P. A. Sleigh and K. G. Kerr, "Development of a numerical model to simulate the biological inactivation of airborne microorganisms in the presence of ultraviolet light," *Journal of Aerosol Science*, vol. 35, pp. 489-507, 2004.

[5] A. C. K. Lai and Y. C. Cheng, "Study of expiratory droplet dispersion and transport using new Eulerian modeling approach," *Atmospheric Environment*, vol. 41, pp. 7473-7484, 2007.

[6] M. A. Camargo-Valero, C. A. Gilkeson, C. J. Noakes and P. A. Sleigh, "An Experimental Study of Natural Ventilation Characteristics and Pathogen Transport in Open and Partitioned Hospital Wards," in *Proceedings of the 9th UK Conference on Wind Engineering*, Bristol, UK, pp.75-58.

[7] D. Etheridge and M. Sandberg, *Building Ventilation Theory and Measurement*, John Wiley & Sons, Chichester, UK, 1996, pp. 6-30.

[8] The American Society of Mechanical Engineers, *Standard for Verification and Validation in Computational Fluid Dynamics and Heat Transfer*, ASME V&V 20-2009, 2009.

[9] B. E. Launder and D. B. Spalding, "The Numerical Computation of Turbulent Flows, *"Computer Methods in Applied Mechanics and Engineering*, vol. 3, pp. 269-289.

[10] P. J. Roache, "Perspective: A Method for Uniform Reporting of Grid Refinement Studies," *Journal of Fluids Engineering*, vol. 116, pp. 405-413.